Japanese Journal of Applied Physics
Vol. 45, No. 6A, 2006, pp. 5332–5343

Development of a Compact Plasma Trap for Experimental Beam Physics

Ryota TAKAI*, Hayato ENOKIZONO, Kiyokazu ITO, Yasuhiko MIZUNO, Kota OKABE† and Hiromi OKAMOTO

Department of Quantum Matter, Graduate School of Advanced Sciences of Matter, Hiroshima University, 1-3-1 Kagamiyama, Higashi-Hiroshima, Hiroshima 739-8530, Japan

(Received January 19, 2006; accepted March 8, 2006; published online June 8, 2006)

A tabletop experimental system has been developed for the study of various collective effects in space-charge-dominated beams. It is based on the recently proposed idea that the dynamic motion of a one-component plasma in a trap can be made physically equivalent to that of a charged-particle beam propagating through a linear transport channel. In this paper, we report on the details of the system and on results of test experiments with a compact Paul trap that is divided into several independent sections. The trap design is carried out in consideration of practical constraints. A Maxwell equation solver is used to calculate the properties of the plasma confinement potential. Experimental observations are compared with numerical data obtained by a tracking simulation code that enables us to approximately predict the three-dimensional trajectories of particles in the system. Low-density N_2^+ plasmas are employed to examine the basic performance of the multi-section trap. The initial temperature, density and lifetime of a confined plasma are estimated from experiments and simulations.
[DOI: 10.1143/JJAP.45.5332]

KEYWORDS: space-charge-dominated beam, one-component plasma, Paul ion trap, collective beam instability

1. Introduction

Charged particle beams generated by accelerators are extremely useful tools with many practical applications. They have now been utilized in a wide variety of fields including fundamental physics, cancer therapy, material sciences, industry, and life sciences. The most important parameter that determines the quality of this tool is the *emittance*. Since a low-emittance beam is generally more useful, we often try to put a large number of particles in a tiny μ-space volume. However, as the phase-space density becomes higher, Coulomb interactions among particles are more enhanced, which may give rise to the serious deterioration of the beam quality. Even if the emittance is moderate, the phase-space density can be rather high in a high-power beam that has attracted increasing interest, e.g., in energy sciences. It is thus essential to clarify the mechanisms of collective instabilities induced by space charges.[1,2)]

The understanding of *space-charge effects* in dense beams has been greatly deepened for the last several decades through extensive theoretical and experimental efforts.[3–24)] Nevertheless, we still have many remaining issues that require further investigation. Theoretically, what we must do is to solve the Vlasov and Poisson equations simultaneously, but the self-consistent treatment of these equations is very difficult especially in the present case where the beam is subject to complex time-dependent external forces. In order to gain better information about the beam behavior, numerical techniques have often been employed. Reliable simulations are, however, quite time-consuming even with the help of modern computers. Substantial difficulties are also encountered in experiments. Since beams are traveling at great speed in the laboratory frame, it is always troublesome to carry out high-precision measurements. In addition, the poor controllability of lattice characteristics and beam quality prevents us from surveying a wide parameter space.

Recently, Okamoto and Tanaka have proposed a novel experimental method to resolve these practical difficulties in conventional approaches.[25,26)] The method is based on the mathematical equivalence between the collective motion of a charged particle beam and that of a nonneutral plasma in a trap system. Two different types of trap configurations, i.e., a radio-frequency quadrupole trap (Paul trap) and a solenoidal trap, were considered as a possible tabletop device to which this idea can readily be applied.[25,26)] The same idea was reemphasized later by Davidson *et al.*[27)] who actually constructed a linear Paul trap for the study of intense beam dynamics. The dedicated plasma trap at the Princeton Plasma Physics Laboratory has already produced some initial experimental results.[28)] Another challenging experimental project is in progress at Maryland University where a compact electron storage ring has been built.[29)]

At Hiroshima University, a prototype system "S-POD (Simulator for Particle Orbit Dynamics)" has been constructed to verify the proposed idea and to demonstrate the practicability of the new experimental scheme.[30)] It is a compact experimental tool composed mainly of a nonneutral plasma trap, a plasma density controller such as a laser cooler, AC and DC power generators, an ultrahigh-vacuum system, and plasma diagnostic systems.[25,26,31)] From two types of possible trap configurations, we chose a linear Paul trap, taking into account its direct correspondence to beam transport channels. The Paul ion trap[32,33)] is a very popular device and has actually been employed for various experimental purposes associated with frequency standards, Coulomb crystals, quantum computing, high-accuracy spectroscopy, and other applications.[34–42)] In these typical applications, a relatively small number of ions are commonly used. In the cases of interest to us here, however, it is preferable to confine as many particles as possible. We have, therefore, developed a unique Paul trap axially separated into several independent sections for plasma conditioning.

In this paper, the details of this "multi-section" Paul trap and its fundamental properties clarified by initial experiments are reported. In §2, we outline how S-POD works and what kinds of beam-dynamics studies can be done with it. We then explain, in §3, the design concept of our Paul trap and, in §4, a three-dimensional (3D) particle tracking code developed for simulating the motion of confined ions. The

*E-mail address: takai@hiroshima-u.ac.jp
†Present address: High Energy Accelerator Research Organization, 1-1 Oho, Tsukuba, Ibaraki 305-0801, Japan.

experimental setup and parameters adopted for test measurements are described in §5. Section 6 is devoted to showing some experimental results that demonstrate the performance of our trap. We also discuss an essential modification of the trap geometry for improving the efficiency of plasma transport. Finally, a summary and future plans are given in §7.

2. S-POD

Among diverse collective effects, we are particularly interested in instabilities directly caused by interparticle Coulomb forces. This type of effect is understood to be a major issue that may essentially influence the basic designs of high-power or high-quality ion accelerators. For instance, any storage ring must be operated in a *resonance-free* region that depends on the beam density. It is also crucial to know the mechanism of halo formation because the uncontrollable loss of tail particles may lead to excessive radio-activation of high-power machines. S-POD allows us to explore these important space-charge effects without relying on a large-scale accelerator system; we can prove that there is a clear analogy between a single-species plasma in a Paul trap and a charged-particle beam in an accelerator.[25,26)]

In order to conduct a systematic investigation into typical space-charge-induced instabilities, several key parameters must be adjustable. The phase advance of the betatron motion and tune depression are especially important in transverse beam dynamics studies. The control of the *bare* betatron phase advance σ_p per unit lattice structure can easily be achieved in a Paul trap through rf parameters. By changing either the rf amplitude V_{rf} or frequency f (or both), we can vary the betatron phase advance over a wide range. In contrast, the precise control of the tune depression η is much more difficult. The definition of this parameter is $\eta = \sigma/\sigma_p$, where σ is the *space-charge-depressed* betatron phase advance per lattice period; the tune depression thus ranges from 0 (space-charge limit) to 1 (high-temperature limit). The amount of the tune shift $\sigma_p - \sigma$ depends on the phase-space density of the plasma, which means that some dissipative process is necessary to change η. For future experiments, we are now developing a laser cooling system to manipulate the thermal motion of a $^{40}Ca^{+}$ plasma. Since the Doppler cooling limit is even lower than the milli-Kelvin order,[43,44)] it is possible to adjust the tune depression to any desired value. Note that the application of the laser cooling technique is beneficial not only to controlling η but also to observing a plasma profile. Since each ion excited by a laser light emits a photon when coming back to the original level, we can perform very high precision, nondestructive measurements by detecting the fluorescence photons.[45)]

Figure 1 displays a stopband distribution obtained from a linearized Vlasov analysis for coasting beams in a FODO channel.[6)] σ_p has been chosen to be 100°. We recognize that linear and nonlinear resonances may be excited only within specific regions of tune depression. The distribution of these *stopbands* is altered once a different choice of σ_p or lattice structure is made. Since the tune depression η is adjustable by laser cooling, we can explore the parameter dependence of resonant instability, thus testing the reliability of various theoretical models. For the study of halo formation, an additional pulse voltage is launched to the electrodes at a certain moment in order to disturb the plasma intentionally. Since the magnitude of the pulse disturbance is controllable, we can systematically investigate the roles of mismatch factor, tune depression, and lattice characteristics in halo formation. As discussed in ref. 31, space-charge effects in bunched beams are also within the scope of the present experimental scheme.

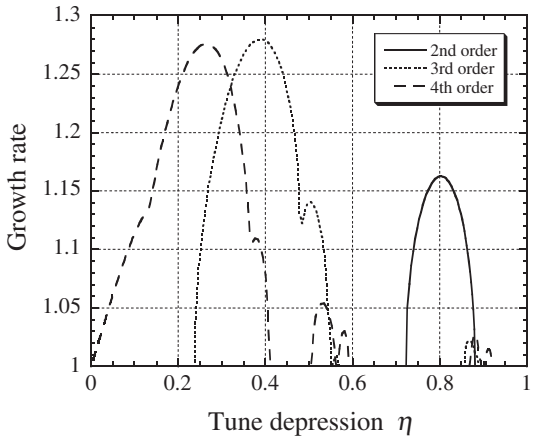

Fig. 1. Transverse stability diagram obtained by linearized Vlasov analysis. The growth rate of resonant beam instability has been plotted as a function of tune depression η. We have considered FODO focusing with 50% filling factor. The bare betatron phase advance per unit cell, σ_p, has been adjusted to 100°. An almost identical stopband distribution can be found even when the external focusing force varies sinusoidally.

S-POD experiments have some practical limitations. For instance, the collective beam instability induced by various wake-field sources[46)] cannot be reproduced in this system. As already emphasized, S-POD is particularly useful for the study of self-field effects that often cause trouble in beams of relatively low energy. We should also bear in mind that the motion of trapped particles is free from momentum dispersion. This means that we cannot look into dynamic effects in which bending magnets play an essential role. One such example is *beam crystallization*. The stability property of "regular" Coulomb crystals in a dispersionless environment has been known much simpler than that of crystalline beams in a storage ring.[47,48)]

3. Design of a Multi-section Paul Trap

3.1 Basic parameters

The prototype of a Paul trap for S-POD is composed of three planar electrodes and two sets of quadrupole rods as illustrated in Fig. 2. Nonneutral plasmas are confined in "Ion Source (IS)" and/or in "Experiment Region (ER)". The thin cylinder between IS and ER is called "Gate" where a static voltage is applied to separate IS and ER. The cylinders at both ends are placed for axial plasma confinement. We call the end electrode of the IS side "Cap A" and the other of the ER side "Cap B". The thickness of these electrodes is 7 mm and their aperture size is $2R$, where R is equal to the minimum distance from the trap axis to the surface of the quadrupole rods. As explained later, the Gate electrode has now been replaced by a short quadrupole to minimize particle loss during plasma transport (see Fig. 11).

The size of the electrode rods is determined through practical considerations, such as the efficiencies of cooling and fluorescence measurement, and the possible range of

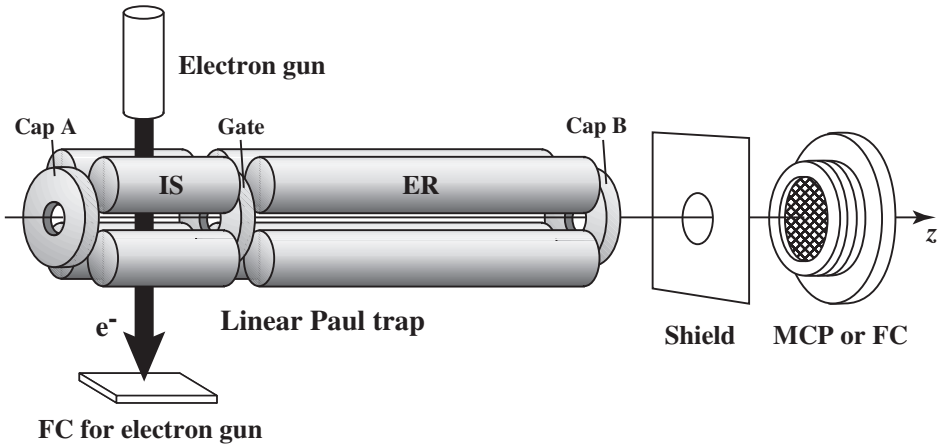

Fig. 2. Schematic view of the trap system.

experimental parameters achievable with a moderate rf power. Although semiconductor lasers are usable to cool a $^{40}Ca^{+}$ plasma, the available power is rather limited. The transverse extent of the plasma should, therefore, be sufficiently small to ensure effective cooling. Considering the power of a commercial ultraviolet semiconductor laser, the reasonable size of a plasma core is, say, a few mm or less. The rms radius a_0 of a stationary plasma column can approximately be given by[31)]

$$a_0 = \frac{c}{\sigma_p f}\sqrt{\frac{Nr_p}{2} + \frac{k_B T_\perp}{mc^2}}, \quad (1)$$

where N and $T_\perp$ are the line density and transverse temperature of the plasma, c is the speed of light, r_p is the classical radius of the particle that has rest mass m and charge state Q, and k_B is the Boltzmann constant. Specifically, we can produce a tiny plasma simply by increasing the rf frequency f. The rf amplitude required for a specific value of σ_p, however, becomes greater at a higher frequency, which yields more rf backgrounds. The use of a lower rf voltage is thus preferred to keep the absolute noise level as low as possible. As is clear from Fig. 3, a smaller R is better in this regard because we can reduce the required amplitude while holding the frequency relatively high (Note that the phase advance is proportional to V_{rf}/R^2 under the smooth approximation). In addition, too high an rf voltage makes it difficult to design a pulse-power generator that emulates the magnetic lattice structures of accelerators. After these practical considerations, we constructed several linear traps with an aperture radius R of less than 10 mm. In what follows, we only discuss recent results based on a prototype with $R = 5$ mm. Once the size of R is given, the radius ρ of the electrodes is automatically determined from the condition for minimizing nonlinear components in the rf field. According to previous numerical calculations,[31,49)] the nonlinearity of the plasma confinement field is most suppressed when $\rho/R \approx 1.15$; the optimum value of ρ is thus 5.75 mm (11.5 mmϕ) for $R = 5$ mm. Provided that $^{40}Ca^{+}$ ions are confined at the frequency of 1 MHz, the rf amplitude of 100 V suffices for realizing $\sigma_p = 153^\circ$. Since the required voltage becomes greater at a higher frequency, the trap has been operated at 1 MHz or less so far. The transverse dimension of a plasma core is then expected to be on the order of a few mm, appropriate for laser cooling. We have

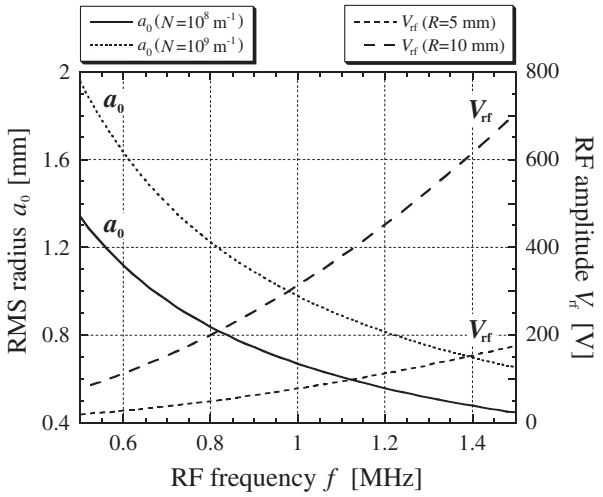

Fig. 3. Estimated rms radius a_0 of confined plasma and required rf amplitude V_{rf}. We have assumed $^{40}Ca^{+}$ ions confined by the pulse voltage emulating a FODO lattice with a 50% filling factor. The betatron phase advance σ_p and the transverse plasma temperature $T_\perp$ have been chosen to be 100° and 0.5 eV, respectively.

developed an rf power supply system that is computer controllable and can generate various pulse voltages imitating beam transport channels of different designs.

The spatial profile of a stationary plasma depends on the axial length of the quadrupole electrodes. Using short rods whose length is comparable to the aperture size $2R$, we can make the longitudinal confinement potential more or less parabolic. Then, the plasma profile becomes an approximate ellipsoid whose aspect ratio can be modified to some extent by changing the rod length. A wider range of the aspect ratio is realizable in the multi-segmented Paul trap described in ref. 31. Provided that the rods are much longer than $2R$, a roughly uniform plasma column can be formed because the bias potentials on the end electrodes are shielded by the rods. The axial lengths of IS and ER of the current trap are 50 and 150 mm, respectively.

3.2 Plasma conditioning

Ideally, we must provide a pure single-species plasma consisting of a large number of particular ions. This is a primary reason why our trap has been divided into two

sections. The main roles of IS are the production and conditioning of an initial plasma that is relocated later in ER. A specific species of positive ions is generated by ionizing neutral particles from an atomic oven with a low-energy electron beam. The oven and electron gun have been installed beside IS. Above IS, there is a spare port reserved for buffer gas cooling. While the electron beam ionizes not only Ca atoms from the oven but also residual gases inevitably, it is an easy matter to remove unnecessary ion species; as is well-known, an rf quadrupole works as a mass filter when proper DC voltages are added to the electrodes. After initial plasma conditioning, ions are transferred into ER where diverse space-charge experiments are executed. The multi-section trap is also convenient for matching the plasma distribution in ER. Since IS and ER are almost independent, we can reduce backgrounds that may be induced by the noise sources in IS, such as the oven, electron beams, and buffer gas. Furthermore, the laser cooling force can be utilized to establish an approximate stationary state; for instance, it is possible to remove tail particles generated during the ionization and stacking process, if necessary.

If the number of ions transported and trapped in ER is not enough for an intended experiment, we repeat the above procedure until the ion number reaches a desired level. There are several practical schemes to do this "plasma stacking" in S-POD. One possible stacking sequence is illustrated in Fig. 4. First of all, we set the base potential of IS slightly higher than that of ER by biasing the quadrupole rods [Fig. 4(a)]. After producing a single-species plasma in IS, we open the Gate potential to move it toward ER. Most particles then go back and forth in the axial direction if no energy dissipation is there [Fig. 4(b)]. We, therefore, apply a cooling laser to decelerate the individual ions, so that they can no longer enter the IS region [Fig. 4(c)]. Finally, the bias voltage at Gate is turned on again for further stacking. Although the ion plasma in ER is heated in every stacking sequence, the heating will cause no serious problem because the axial motions of hot ions are repeatedly cooled by the laser. We rather anticipate that fast ions from IS may be sympathetically decelerated through collisions and thus accumulated in ER. The final control of the plasma temperature is carried out by the Doppler cooling method after the number of ions in ER reaches a sufficient level. The unit stacking cycle can be completed very quickly; it takes much shorter than the lifetime of the plasma. It is thus possible, in theory, to accumulate a large number of specific ions in ER.

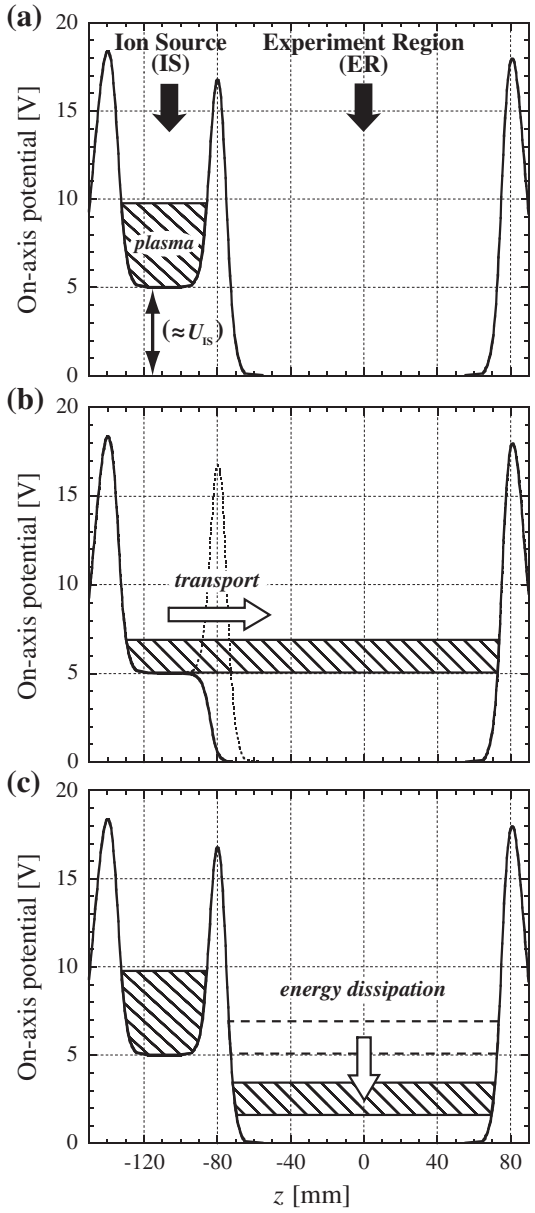

Fig. 4. A possible scheme for plasma stacking. First of all, the potential barrier is removed to transport a nonneutral plasma in IS toward ER. We then introduce some dissipative interactions (e.g., a laser cooling force) to decelerate individual ions. After the completion of a plasma transport, the bias voltage of Gate is switched on again for further stacking. This process is repeated at a cycle much shorter than the lifetime of the plasma. The base potential in IS is controlled by applying the bias voltage U_{IS} to the quadrupole rods.

4. 3D Tracking Simulations

In order to interpret various experimental data precisely, we have developed a particle tracking code that three-dimensionally analyzes the motion of an ion in an arbitrary trap configuration. The Maxwell equation solver "MAFIA"[50] is employed to evaluate the distribution of the electric potential in the system including the trap, rf shields, electron gun, and other elements. Since the rf wavelength considered in the present experiments is much longer than the overall dimensions of the trap system, it is allowed to apply the static-field approximation. The potential data given at 3D mesh points in a given structure are input to the tracking code for particle trajectory analysis. Coulomb interactions among confined particles are currently ignored for quick simulations, which should be acceptable at this stage where we have no intention of trapping a large number of ions. Only low-density plasmas have been used in most experiments so far because the primary task is to understand the fundamental features of S-POD for future beam-dynamics studies.

For meaningful comparison with experimental observations, a proper initial distribution of particles must be assumed in each simulation. It is, however, difficult to know the exact phase-space profile of a confined plasma until a laser-induced-fluorescence (LIF) diagnostic becomes available.[45] In fact, ions are randomly produced everywhere in IS

through interactions with electrons deflected by the rf field continuously. We thus took the following procedure to figure out a possible particle distribution for tracking study: As to the transverse degrees of freedom, 100 particles are randomly generated within a circle of radius R at every 5 ns (corresponding to 1/200 of an rf period). All these particles are initially located in the middle of the IS region because the electron gun is sitting there. The momentum distributions are chosen to be Gaussian in all three degrees of freedom. We repeat this particle generation process for an rf period. Since we have neglected the Coulomb coupling among particles, the standard deviations of the transverse and longitudinal momentum distributions are not necessarily equal even after many rf periods. The amount of momentum spread in the longitudinal direction was determined so as to reproduce experimental results. As shown later, the initial longitudinal temperature is most likely to be about 0.3 eV at low line density. The transverse plasma temperature after a short storage is insensitive to the input standard deviation; heating from the rf field determines the thermal energy in this direction. In case $^{28}N_2{}^+$ ions are confined with the rf amplitude of 42 V at the frequency of 1 MHz, systematic simulations suggest that the transverse temperature should initially be around 0.6 eV. This is comparable to 10% of the effective potential depth. The average transverse rms extent of the plasma is then 2.2 mmϕ under the smooth approximation. Figure 5 shows the typical distribution of ions 100 ms after the particle generation procedure above was completed. Since an rf field is applied, the transverse plasma profile rapidly oscillates in time. The total number of surviving particles is about 4300 in this example. The longitudinal temperature has somewhat decreased from the initial value because the survival time of a higher-energy particle tends to be shorter. The loss of high-energy particles also leads to a rapid decrease in transverse temperature in the early stage of a plasma storage (see Fig. 15). The simulation results in §6 have been obtained assuming this initial distribution.

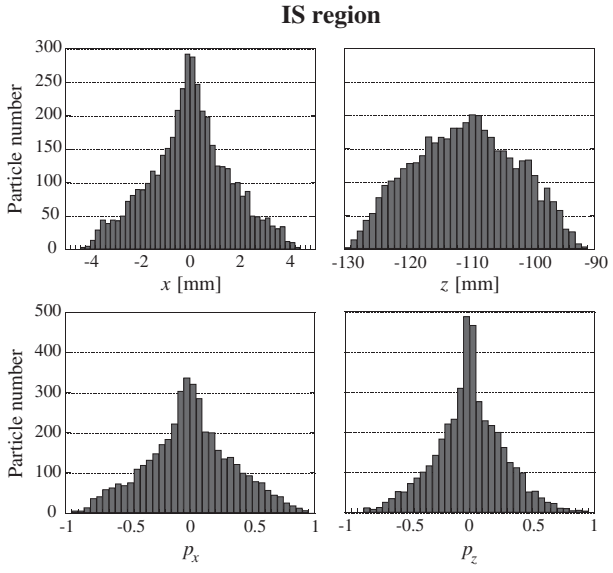

Fig. 5. Initial particle distribution employed in 3D particle tracking simulations. The rf amplitude and frequency of IS have been set at 42 V and 1 MHz. $p_{x(z)}$ denotes the scaled horizontal (longitudinal) momentum.

5. Experimental Setup

5.1 Outline

The arrangement of main components in a vacuum chamber has been depicted in Fig. 2. A turbo-molecular pump (Seiko Seiki, STP-300T) is employed to maintain a high vacuum of under 5×10^{-7} Pa. An electron gun (Toshiba Hokuto Electronics, FM2282-A5) mounted above IS produces a well-focused electron beam to ionize neutral atoms in the IS region. The beam current can be monitored with a Faraday cup (FC) at the opposite side of the electron gun. Since we eventually need to trap laser-coolable ions, a compact atomic oven has been installed beside IS. In the present initial experiments, however, the oven was not turned on; we simply used $^{28}N_2{}^+$ plasmas generated from residual gases.

We have performed a number of test experiments, trying various combinations of electrode potentials. Typically, the base potential of the IS region is chosen to be several volts higher than that of ER by biasing the quadrupole rods in IS, in order to accelerate particles toward the detector (see Fig. 4). The bias voltage applied to IS is denoted by U_{IS} in the following.[51] As an ion detector, we have used either a FC or a microchannel plate (MCP). In the case of FC measurements, ion loss between Cap B and the FC can be reduced considerably with a high U_{IS}. The loss rate is much lower in MCP measurements due to a high negative voltage on the front surface of the MCP. The heights of the longitudinal potential barriers relative to the U_{IS} level have been adjusted to less than 20 V. During an ionization process in IS, the DC voltage on Gate is usually set to be equal to the Cap-A potential. The electron gun is switched on for 5 to 10 s to ionize residual gases.

5.2 Operating point of the trap

As mentioned above, our rf power generator can produce a wide variety of pulse waveforms emulating different beam-focusing lattices. We have, however, presently employed the conventional sinusoidal waveform for the sake of simplicity.[52] The transverse motion of charged particles confined with the rod voltages of the form $\pm(U + V_{rf}\cos\Omega t)$ is governed by the Mathieu equation:[32,33]

$$\frac{d^2u}{d\xi^2} \pm (a + 2q\cos 2\xi)u = 0, \tag{2}$$

where u represents one of the transverse coordinates (x or y), $a \equiv 8QU/(mR^2\Omega^2)$ and $q \equiv 4QV_{rf}/(mR^2\Omega^2)$ are the Mathieu parameters, $\xi \equiv \Omega t/2$ is the dimensionless independent variable, and we have ignored the Coulomb potential. The a-parameter is set to be nonzero for mass filtering. According to the Floquet theorem, there must be a solution of the form $u(\xi) = w(\xi)\exp[i\psi(\xi)]$, where the amplitude function $w(\xi)$ and phase function $\psi(\xi)$ have a periodicity identical to that of the focusing function $K_{rf}(\xi) = a + 2q\cos 2\xi$. Substituting the Floquet solution into eq. (2), we obtain the differential equation for $w(\xi)$

$$\frac{d^2w}{d\xi^2} \pm K_{rf}(\xi)w - \frac{1}{w^3} = 0, \tag{3}$$

where the normalization $d\psi/d\xi = 1/w^2$ has been taken. Equation (3) is usually referred to as the *envelope equation*

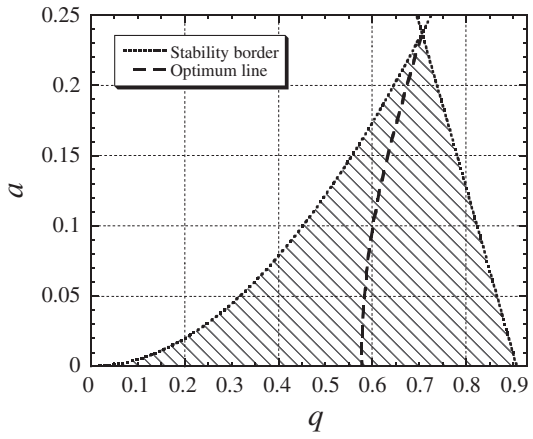

Fig. 6. Optimum operating line along which the transverse plasma extent becomes the smallest (broken line). Equation (3) has stable periodic solutions in the hatched area.

in beam dynamics theories.[1)] The stability of the periodic solution is often explained with the (q, a) diagram. The maximum amplitude of w, in other words, the transverse extent of the plasma core depends on where the operating point of the system is located on the diagram. Since the plasma is more expanded near the stability border, the operating point should be chosen deep inside the stability region so as to maximize the number of confined ions. In order to identify the best parameters, we numerically integrated eq. (3) with possible combinations of q and a. We then found Fig. 6 in which the optimum operating conditions have been indicated with a broken line. When $a = 0$, the plasma core is expected to be most compact at $q \simeq 0.58$. This corresponds to the vacuum phase advance of 79°. The optimum rf amplitude is thus 42 V for $^{28}N_2{}^+$ ions at the frequency of 1 MHz. This combination of the rf parameters ($V_{rf} = 42$ V and $\Omega/2\pi = 1$ MHz) has been adopted for experiments reported in the subsequent sections.

The numerical estimate made here is relevant only in an emittance-dominated regime. The optimum parameters could be different at higher density where the space-charge potential dominates the plasma. It is also worthy to note that, even if the Coulomb interactions are negligible, the number of ions in the trap is not always maximum under the operating conditions derived above; it more or less depends on the initial distribution of particles according to tracking simulations. For instance, the rf amplitude (or q-value) that maximizes the ion number after a short storage is smaller than the value expected from the broken line in Fig. 6 if we uniformly distribute particles within the whole confinement region (i.e., the circle of radius R) at the beginning. Another noteworthy factor is nonlinear resonances induced by imperfection fields.[53,54)] As long as we employ cylindrical electrodes, the transverse confinement force inevitably contains higher-order multipole components that may limit the storage time of ions when a and q satisfy specific conditions.

5.3 Detectors

Either a MCP (Hamamatsu Photonics, F4293-24) or a FC, movable along the axial direction, has been utilized to count the number of ions. The MCP is placed 25 mm away from Cap B. A current gain of higher than 10^6 can be attained when secondary electrons have a kinetic energy above 1.5 keV. We have applied a negative voltage of 2 kV to the front surface of the MCP in order to accelerate ions from the trap. Since such a high voltage can seriously affect the plasma confinement potential near the MCP, we have placed an aluminum shielding plate to minimize the potential distortion in ER. The aperture size of the shield is 13 mmϕ. The location and design of the shield have been carefully optimized through particle tracking simulations as well as MAFIA calculations. Owing to the high negative potential that attracts ions, almost no particle loss is caused by the shield.

While the MCP has a very high sensitivity, its gain starts to degrade once the output current exceeds 5–10% of the strip current.[55–58)] The magnitude of an output signal is then not proportional to the total number of incident ions. The MCP is, therefore, suitable for measuring *thin* plasmas. In contrast, a large number of ions are needed in FC measurements because of the FC's much lower sensitivity. The output signal is, however, simply proportional to the total current regardless of the number and spatial distribution of charged particles. We have thus used the FC, instead of the MCP, whenever the number of confined ions is expected to be large.

Since no high bias voltage is applied unlike in the case of the MCP, the FC should be positioned as close to the trap as possible; otherwise, many particles cannot reach the FC, which may considerably diminish the magnitude of the output signal. In order to evaluate the transverse plasma spread in the drift space after Cap B, we performed 3D tracking simulations. The standard deviation s_p of the transverse particle distribution is plotted in Fig. 7 as a function of the longitudinal coordinate. In this example, $U_{IS} = 10$ V, and the modified Paul trap described later in §6.2 has been assumed (see Fig. 11). The divergence angle can be made smaller by increasing U_{IS}. Provided that the shield box is fixed as close to the end electrode as possible, the aperture of at least 15 mmϕ is necessary to let almost all ($\pm 3s_p$) of the output particles pass through the shield hole. The dimension of the FC should be large enough to collect all these particles. Obviously, the required dimension can be reduced by placing the FC closer to the shield. We then have to resolve noise problems that become severer as the distance to ER becomes shorter. The most severe noise to the FC comes from switching on and off the DC potential of Cap B, rather than the rf field in ER. To increase the signal-to-noise (SN) ratio, we made a rough estimate of the switching noise, employing the MAFIA code. It was found that the SN ratio is improved by distancing a larger FC from Cap B. We finally decided to locate the FC of 30 mmϕ at the position indicated by the broken line in Fig. 7.

6. Experimental Results

6.1 Preliminary measurements

6.1.1 Mass spectrum

As is well-known, a Paul trap works as a mass filer once the DC voltage U on the quadrupole electrodes, in other words, the a-parameter in eq. (2) is switched on. The operating point for the target ion species must then be near the broken line in Fig. 6. In order to confirm that we can

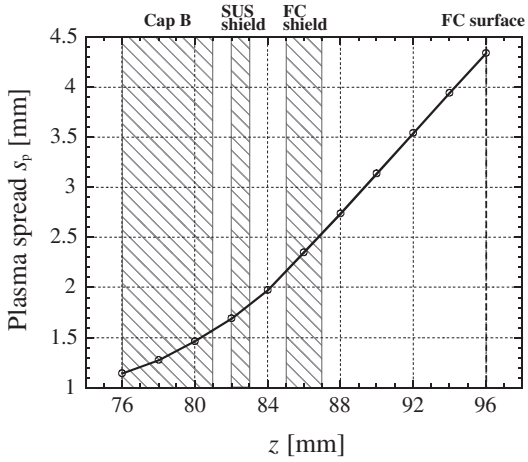

Fig. 7. Transverse plasma extent evaluated by a 3D tracking simulation. The standard deviation of the transverse particle distribution after the plasma is extracted from the Paul trap is shown. The three hatched areas indicate the regions where Cap B, a grounded shielding plate made of SUS, and the shield box for the FC are located. We have assumed $^{28}N_2{}^+$ ions accelerated with $U_{IS} = 10$ V.

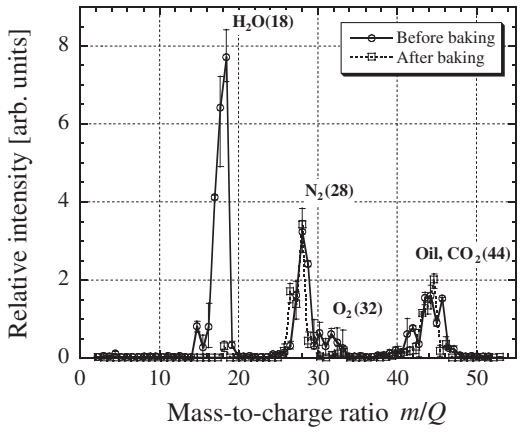

Fig. 8. Mass spectra of residual gasses before and after the baking of the vacuum chamber.

actually select ion species, test experiments were executed. The measured mass spectra of residual gases in the chamber are displayed in Fig. 8. We can convert the applied rf and DC voltages into mass-to-charge ratio m/Q, assuming that the number of specific ions becomes maximum along the broken line in Fig. 6. As expected, the spectrum taken before the baking of the chamber has a sharp peak at $m/Q \approx 18$ amu/charge state corresponding to H_2O^+ ions. After a 60-hour baking, this peak was gone. The second pronounced peak, not affected by the baking, should be due to $^{28}N_2{}^+$ ions. Figure 8 shows that it is possible to separate laser-coolable ion species produced in IS, if necessary.

6.1.2 *Efficiency of plasma transport*

Using the first prototype in Fig. 2, we examined how efficiently ions can be transported from IS to ER. The initial setting of DC potentials is similar to that illustrated in Fig. 4(a); namely, the base potential of the IS region is set higher than the ground level of ER by the bias voltage U_{IS}, and other planar electrodes (Gate, Cap A and Cap B) create barriers for longitudinal plasma confinement. After a 10-

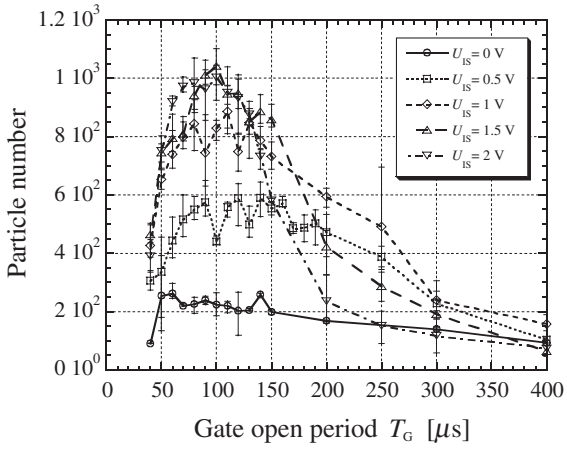

Fig. 9. Results of ion transport experiments with the first prototype (Fig. 2) whose Gate electrode is a thin cylinder.

second ionization process followed by a 1-second storage in IS, we open Gate by switching off the DC bias on it, so the ions flow into ER. The central barrier is quickly reconstructed in the "Gate open period T_G (s)" and we further wait for 10 ms. Finally, the bias on Cap B is turned off to send the plasma toward the MCP detector. The minimum switching time of the bias potentials is a few 100 ns, which is much shorter than T_G. Figure 9 summarizes the results of plasma transport experiments in which five different values of U_{IS} have been tested. We see that the number of detected particles strongly depends not only on U_{IS} but also on T_G.

In order to interpret the result in Fig. 9, systematic simulations were performed taking into account the actual experimental procedure described above. For the sake of simplicity, we assumed all confined ions to be $^{28}N_2{}^+$. The tracking result corresponding to the experiments in Fig. 9 is given in Fig. 10, where the effects of the MCP potential, shielding plate and other elements along the transport line have been incorporated on the basis of MAFIA calculations. The upper picture shows the rate of the ions that finally reached the MCP after a 10-millisecond storage in ER. The simulations have qualitatively reproduced the experimental observation. The number of ions lost in 300 μs after Gate was opened has been depicted in the lower picture as a function of the axial coordinate. In this simulation, $U_{IS} = 1$ V and the initial particle number is about 4300. We recognize that most ions have escaped from the trapping region in the vicinity of the central Gate electrode. This is because ions receive no transverse focusing force within the Gate region. The rapid decrease in transport efficiency for $T_G > 100$ μs can readily be explained by this loss mechanism. With a higher U_{IS}, the loss rate tends to be lower at Gate; the reduction of ion loss near Gate is due to the shortening of the net passage time.

6.2 *Experiments with a modified Paul trap*

6.2.1 *Gate modification*

Responding to the preliminary results with the first prototype, we replaced the planar Gate electrode with short quadrupole rods to prevent the possible particle loss between IS and ER. The rods are 9 mm long and provide a transverse focusing force in addition to the potential barrier for longitudinal plasma confinement. A schematic drawing of

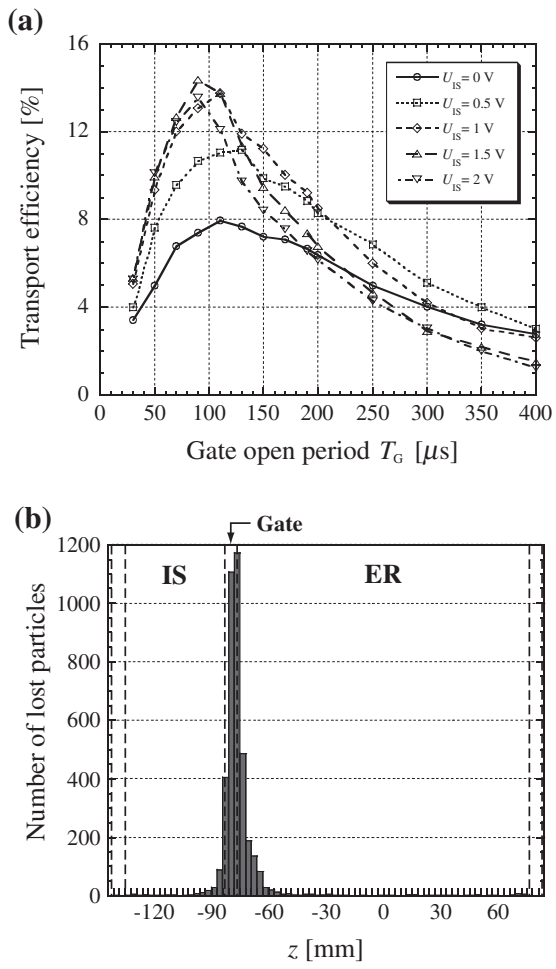

Fig. 10. Simulation results of ion transport experiments with the first prototype in Fig. 2. These simulations have considered exactly the same experimental procedure as taken in the actual experiments in Fig. 9. We have assumed that all ions are $^{28}N_2^+$. (a) Ion transport efficiency as a function of T_G. (b) Number of $^{28}N_2^+$ ions lost in 300 μs after the Gate barrier was removed. The bias potential on the IS electrodes is $U_{IS} = 1$ V in this example. The total number of particles is 4300 initially. Significant particle loss has occurred in the short Gate region where no transverse focusing force is present.

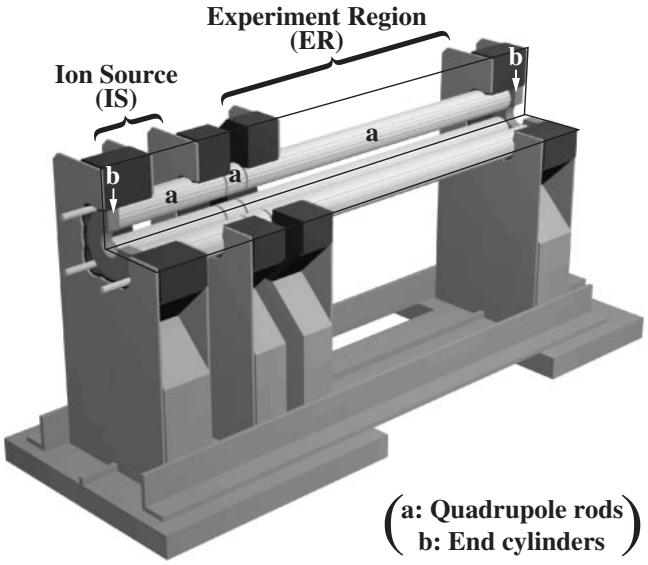

Fig. 11. Schematic view of a modified Paul trap. The planar Gate electrode of the first prototype has been replaced with short quadrupole rods in order to improve the ion transport efficiency.

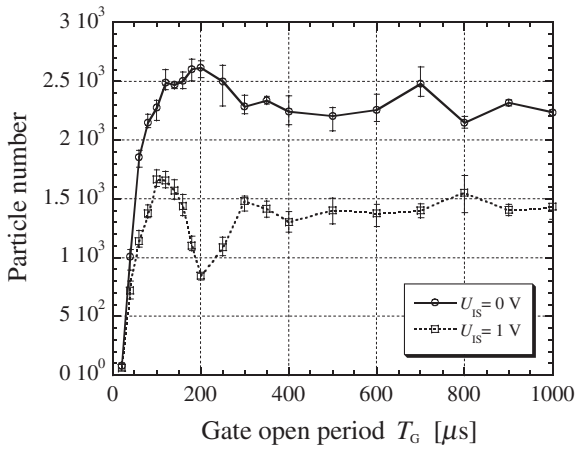

Fig. 12. Results of ion transport experiments with the modified multi-section trap (Fig. 11) whose central Gate is a short quadrupole. The experiments have been performed under the same conditions as adopted for the previous experiments in Fig. 9.

the modified Paul trap is exhibited in Fig. 11. The Gate quadrupole is excited by an independent power supply at the same frequency and amplitude as used for IS and ER. The three sets of quadrupole rods have been carefully spaced 1 mm apart. According to a MAFIA estimation, the effect of such a narrow gap is negligible. We have also changed the thickness of the two end caps from 7 to 5 mm. The ceramic blocks supporting the electrodes have been covered with thin stainless plates that hopefully reduce electric noises to the detector as well as undesirable charges induced on the ceramic surface. All of the following experimental results have been obtained with this modified Paul trap.

6.2.2 Improvement of the plasma transport efficiency

We tested whether the efficiency of plasma transport is actually improved in the modified trap. The measurement data in Fig. 12 were obtained through the same experimental procedure as taken in Fig. 9. Two different bias voltages in IS (i.e., $U_{IS} = 0$ and 1 V) have been considered. The number of ions detected at the MCP increases steadily until T_G becomes long enough for all ions to come out from IS. Unlike the previous result in Fig. 9, the signal maintains an almost constant level for $T_G > 200$ μs without acceleration ($U_{IS} = 0$ V), which strongly suggests that the serious ion loss no longer occurs in the Gate area. A different tendency is observed when $U_{IS} = 1$ V. The signal has a peak at $T_G \approx 100$ μs and, then, comes to a minimum at $T_G \approx 200$ μs. Although the ion number eventually becomes independent of T_G, the signal level is significantly lower than that of the no-acceleration case.

The result of corresponding tracking simulations is shown in Fig. 13(a), which qualitatively explains the experimental observation. When $U_{IS} = 0$ V, a transport efficiency of about 70% is achieved. More than half of the remaining 30% of the ions are not lost but re-trapped in IS after Gate was closed. The "real" loss rate during the plasma transport process is, therefore, much lower. From Fig. 13(b), we can verify that only very little particles are lost inside the trap. The slight

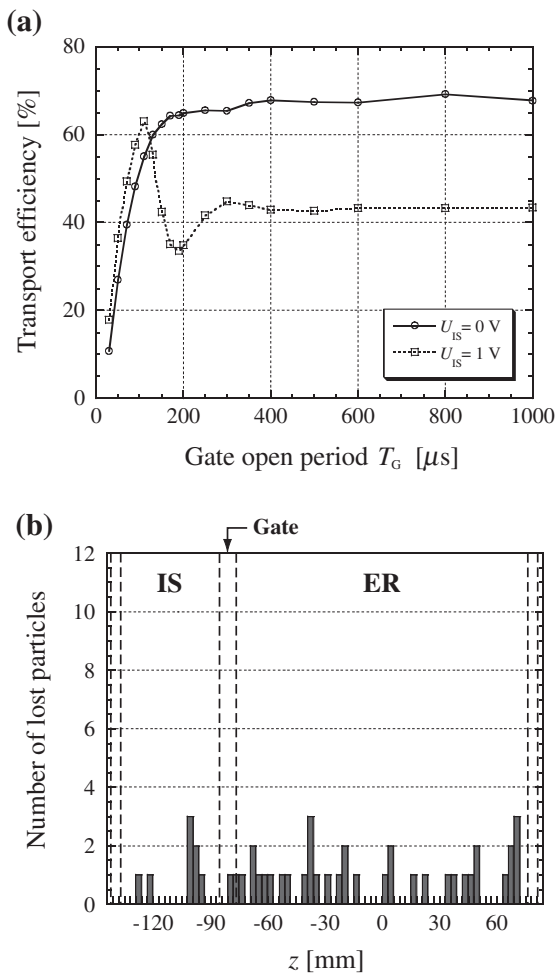

Fig. 13. Simulation results corresponding to the ion transport experiments in Fig. 12. (a) Ion transport efficiency as a function of T_G. (b) Number of $^{28}N_2^+$ ions lost in 300 µs after the Gate barrier was removed. The bias potential on the IS electrodes is $U_{IS} = 1$ V. The total number of particles is 4300 initially.

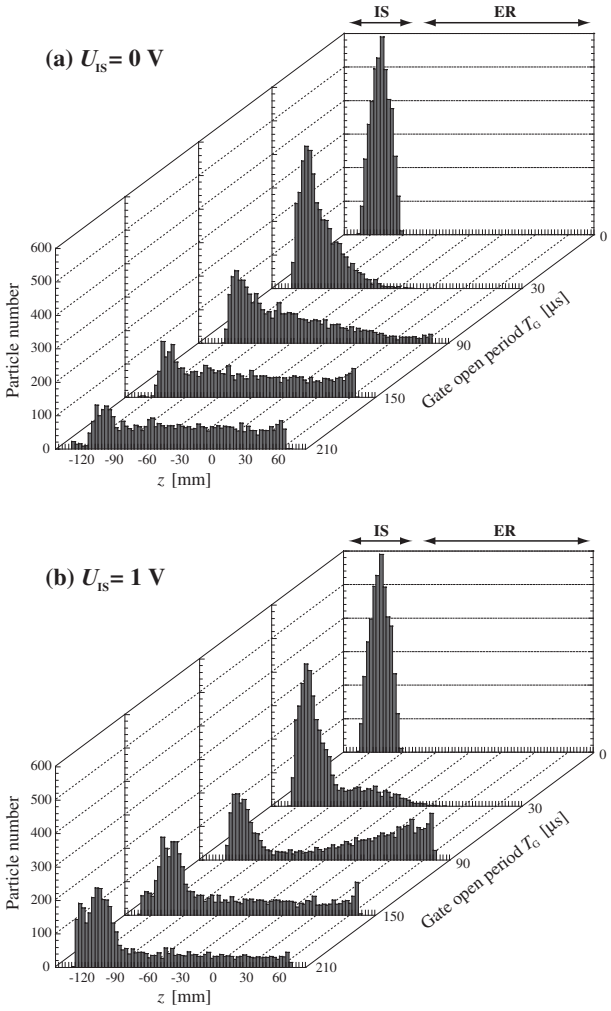

Fig. 14. Time evolution of a longitudinal ion distribution after Gate was opened.

loss is attributed mainly to tail particles of the initial distribution. The simulation results in Fig. 14 help us to understand the experimental data of the $U_{IS} = 1$ V case. The two pictures represent the time evolution of particle population along the trap axis after the Gate barrier was removed. Since no dissipative mechanism is present, each ion goes in and out of ER, and the plasma eventually spreads over the whole confinement region. When $U_{IS} = 0$ V, the axial distribution of ions quickly becomes almost uniform as demonstrated in Fig. 14(a). A clear contrast can be seen in the lower picture where U_{IS} is finite. Owing to the acceleration, we observe, in Fig. 14(b), a cluster of ions moving into ER at $T_G \approx 100$ µs and then coming back to IS at $T_G \approx 200$ µs. This plasma behavior results in the formation of the peak identified in Fig. 12 [or Fig. 13(a)]. After $T_G \approx 300$ µs, the axial ion distribution settles into a nonuniform one similar to the last profile in Fig. 14(b); namely, ions are more populated in IS when U_{IS} is finite. This is because the longitudinal average velocity of the ions is much greater in ER owing to the acceleration by U_{IS} and, as a result, the ions stay in IS for longer periods. The reduction of particle number at a higher U_{IS}, seen in Fig. 12, is caused by this nonuniformity of the axial plasma profile.

6.2.3 Ion storage time

It is important to know how long we can hold a plasma without the major deterioration of its quality. Possible causes that may lead to ion loss include mechanical imperfections and electric noises, collisions with residual gas atoms, Coulomb scattering, recombinations with background electrons, mismatch of the ion distribution to the plasma confinement potential, and nonlinear resonances. To estimate the lifetime of an initial low-density plasma in ER, we measured the number of ions as a function of the storage time. Similarly to the previous experiments, the electron gun was turned on for 10 s. One second after the gun was turned off, Gate was opened for 200 µs to deliver the ions into ER. U_{IS} was set at 0 V in this experiment. Figure 15 shows how an unconditioned plasma in ER decays in time. We see that there are two essentially different time constants; namely, many ions quickly escape from the trap within the first less than 100 s and, after that, the decay rate becomes much lower. Such a behavior of a single-species plasma in a Paul trap has been reported in refs. 59–61. The rapid initial loss is probably due to high-energy ions generated near the edge of the confinement region or, more correctly, outside the dynamic aperture of the system. The primary cause of the slow decay has not been identified yet; possible loss

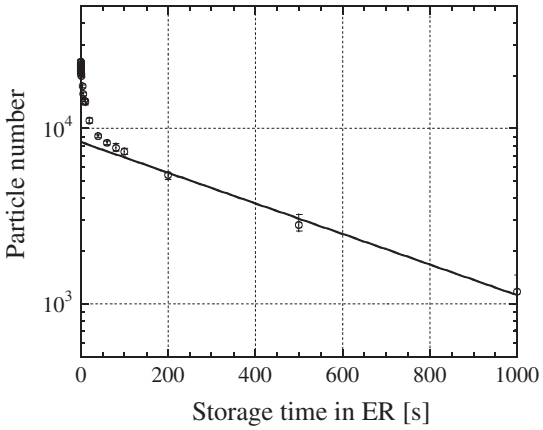

Fig. 15. Number of confined ions vs storage time in ER. The $1/e$ lifetime of the plasma is longer than a few 100 s under the current experimental conditions.

mechanisms include the nonlinear distortion of ion orbits in the vicinity of the end electrodes, and collisions and recombinations with other species of residual particles. The plasma storage time estimated from the slow-decay region is about 500 s corresponding to over 10^8 focusing periods. This is on the same order as (or even longer than) past experimental results with rf traps.[59–65] An analogous result has been obtained in lifetime measurements for IS. We can, therefore, maintain an ion plasma for a period long enough to complete a space-charge experiment.

6.2.4 *Correction to FC outputs*

As explained in §5.3, the number of ions in the trap cannot be accurately measured with the FC because of particle loss in the drift space. Since it is important to find out the ion number as precisely as possible, we estimated the loss rate by comparing experimental and numerical data. For this purpose, the Cap-B potential was kept at the ground level, so ions in IS simply pass through ER without reflection. The ionization time was shortened to 5 s and, after a 10-millisecond storage, the generated ions were released from IS by dropping the DC barrier at Gate. In order to have a better SN ratio, we tried to increase the number of ions by intentionally introducing N_2 gas into the chamber. The U_{IS} dependence of particle number measured with the FC is plotted in Fig. 16(a). The FC outputs have rapidly grown until the accelerating bias voltage U_{IS} reaches about 5 V. Then, the signals are saturated at constant levels depending on the vacuum pressure. This clearly indicates the expected ion loss that occurs between Cap B and the FC. The improvement of the transmission efficiency at higher U_{IS} is, as pointed out in §5.3, due to the reduction of the divergence angle of the plasma envelope in the drift space. The experiments can be simulated using the tracking code with which we have obtained Fig. 16(b). The picture shows the rate of ions that arrive at the FC passing through the hole of the shield box. This simulation result qualitatively agrees with the experimental observation in Fig. 16(a). About 10% ion loss is caused not at the shield box but in the Cap-B area. The gradual decrease in transmission efficiency at higher U_{IS} is attributed to additional loss in the vicinity of the Gate electrodes, which was not observed in the experiments. We

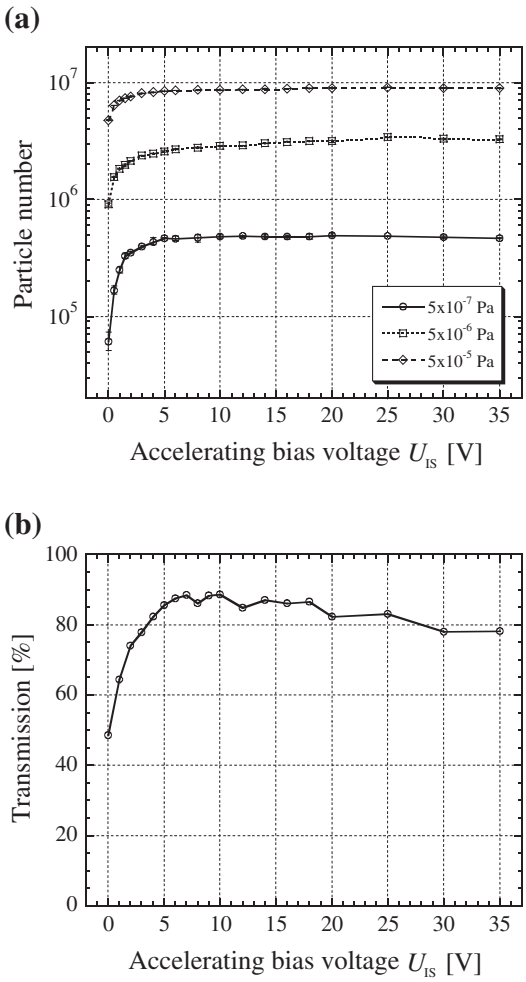

Fig. 16. Dependence of FC outputs on the base potential in IS. (a) Measurement results at different vacuum pressures. (b) Results of 3D tracking simulations.

thus conclude that an output signal from the FC reflects 90% of the actual number of ions in the trap.

6.2.5 *Longitudinal plasma temperature*

The transverse motion of each particle is strongly heated by the rf field as soon as it is ionized in IS. The energy gain from the electric quadrupole field is so large that heating from the rf field determines the transverse temperature $T_\perp$ of the plasma. Assuming the core extent of a few mm, we expect that $T_\perp$ is on the order of 10^3 K because the effective confinement potential at the core edge is around 0.5 V in the present setup. This is consistent with the tracking result in §4. On the other hand, there is no direct heating mechanism in the longitudinal degree of freedom. The axial temperature $T_\parallel$ may, therefore, be rather different from $T_\perp$ as long as the plasma density is low.[66] Tracking simulations have actually revealed that a large temperature imbalance between the transverse and longitudinal directions can be maintained without Coulomb interactions. The longitudinal ion motion is, however, not completely independent of the transverse oscillation. Strictly speaking, the two motions are weakly coupled through electric noises, imperfection fields and nonlinearity near both ends of the confinement region. Coulomb collisions can also be a major source of coupling when the plasma becomes denser.

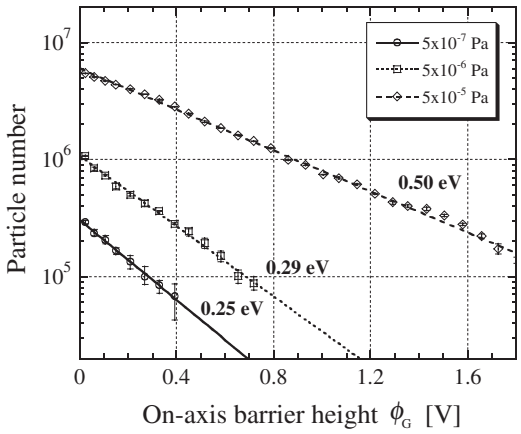

Fig. 17. Results of longitudinal plasma-temperature measurements performed at various vacuum pressures.

It is possible to estimate the longitudinal temperature by adjusting the height of the potential barrier at Gate. In the experiments reported in the previous subsections, we have grounded the Gate potential whenever a plasma is released from IS. Instead, we now switch the potential not to the ground level but to a finite value slightly higher than U_{IS}. Before the switching, the barrier is set 20 V higher than the base potential in IS; namely, during the ionization and plasma storage, the Gate voltage is fixed at $U_{IS} + 20$ V. For longitudinal temperature measurements, this barrier is lowered to $U_{IS} + u_G$ ($u_G > 0$) such that only a high-energy portion of the plasma can escape from IS. Provided that the energy distribution of the plasma is of the Maxwell–Boltzmann type, the number of ions that escaped should approximately be proportional to $\exp(-Q\phi_G/k_B T_\parallel)$, where ϕ_G denotes the height of the *on-axis* Gate barrier relative to the *on-axis* base potential in IS when $U_{IS} + u_G$ ($u_G > 0$) is applied to Gate. $T_\parallel$ can thus be evaluated from the ϕ_G dependence of ion number measured with the FC. Figure 17 shows the results of temperature measurements carried out at various vacuum pressures. We stored plasmas for 10 ms before reducing the Gate potential to $U_{IS} + u_G$. The value of u_G can be converted into the on-axis barrier height ϕ_G on the basis of MAFIA calculations. Considering the observation in Fig. 16, U_{IS} was set at 10 V for all measurements. The ionization time is 5 s. The linear fitting of each data leads to the longitudinal temperature as follows: 0.25 eV for 5×10^{-7} Pa, 0.29 eV for 5×10^{-6} Pa, and 0.50 eV for 5×10^{-5} Pa. As expected, $T_\parallel$ is lower than $T_\perp$ estimated above and becomes higher at poorer vacuum due to more Coulomb interactions and collisions with background atoms.

Taking into account the 10% particle loss in the drift space (Fig. 16), we have successfully confined 10^7 ions in IS. The longitudinal temperature is then 0.5 eV. At this temperature, the approximate longitudinal extent of the plasma should be 35 mm according to a MAFIA estimation of the potential well along the trap axis. The average line density achieved is, therefore, $N \approx 3 \times 10^8$ m^{-1}. If we take the transverse temperature of 0.6 eV numerically evaluated in §4, eq. (1) gives $a_0 \approx 1.2$ mm and the corresponding tune depression is 0.86. The total number of ions, after being transported from IS to ER, rapidly decreases in a few tens of seconds as demonstrated in Fig. 15. We can, however, recover or even increase the line density by the plasma stacking technique outlined in §3. By employing laser cooling, the volume density can easily be improved to a level appropriate for various space-charge experiments.

7. Summary

We have developed a tabletop experimental system that enables one to conduct a systematic experimental study of collective beam dynamics. The system, which we call S-POD, consists of a compact nonneutral plasma trap, an ion source, a variety of power supplies, a laser cooler that is also usable as a diagnostic tool, charged-particle detectors, and vacuum instruments. As a possible plasma confinement apparatus, we adopted a Paul ion trap and constructed several prototypes. A 3D Maxwell equation solver was employed to determine the dimensions of trap components. For convenience in future space-charge experiments, our trap has been designed such that a couple of potential wells can be formed in the axial direction. Such a "multi-section" trap is useful for ion-species selection, noise reduction, plasma stacking and conditioning. Through test experiments, a minor modification was made to the first prototype to minimize ion loss in the Gate region. The current Paul trap (Fig. 11) has allowed us to achieve a plasma transport efficiency of nearly 100%. A 3D particle tracking code has also been developed to understand experimental observations as precisely as possible.

We have studied the basic system performance including the ion storage time, initial plasma temperature, the number of confinable ions, mass filtering, and the influences of bias potential and vacuum pressure. $^{28}N_2^+$ ions generated from residual atoms have been used for this purpose. The typical storage time of our trap is about 500 s after a rapid decay of tail particles in the first 100 s (Fig. 15). The longitudinal plasma temperature is less than 0.3 eV at a high vacuum ($<10^{-6}$ Pa), while it increases to 0.5 eV at 5×10^{-5} Pa. Although the transverse temperature cannot be directly measured with the present diagnostic system, it is possible to estimate it because heating from the rf field is the most dominant energy source in that direction. Tracking simulations suggest that $T_\perp$ should initially be around 0.6 eV, which is somewhat greater than $T_\parallel$. This value is expected to decrease to near 0.5 eV in several tens of seconds due to the loss of tail particles. The maximum line density reached in IS without plasma conditioning is $N \approx 3 \times 10^8$ m^{-1}, corresponding to a tune depression of 0.86. We are now constructing a laser cooler in order to control the plasma density over a wide range. The laser system is important not only for cooling but also for LIF measurements, plasma stacking and matching. An atomic oven is ready to produce $^{40}Ca^+$ plasmas coolable with semiconductor lasers. Test experiments of plasma stacking will start hopefully in a year.

Acknowledgements

The authors would like to thank Dr. Iwashita for valuable discussions on the rf power amplifiers. They are also indebted to Drs. Urabe and Toyoda for useful information on laser cooling systems. This work was supported in part by a Grant-in-Aid for Scientific Research from the Ministry of Education, Culture, Sports, Science and Technology.

1) See, for example, M. Reiser: *Theory and Design of Charged Particle Beams* (Wiley, New York, 1994), and references therein.
2) *Space Charge Dominated Beams and Applications of High Brightness Beams*, ed. S. Y. Lee (AIP, New York, 1995) AIP Conf. Proc., Vol. 377.
3) F. Sacherer: Lawrence Berkeley National Laboratory Report No. UCRL-18454, 1968.
4) R. L. Gluckstern: Proc. Linac Conf., Fermilab, Batavia, IL, 1970, p. 811.
5) R. A. Jameson: IEEE Trans. Nucl. Sci. **28** (1981) 2408.
6) I. Hofmann, L. J. Laslett, L. Smith and I. Haber: Part. Accel. **13** (1983) 145.
7) J. Struckmeier and M. Reiser: Part. Accel. **14** (1984) 227.
8) J. M. Lagniel: Nucl. Instrum. Methods Phys. Res., Sect. A **345** (1994) 46.
9) M. Venturini and R. L. Gluckstern: Phys. Rev. STAB **3** (2000) 034203.
10) H. Okamoto and K. Yokoya: Nucl. Instrum. Methods Phys. Res., Sect. A **482** (2002) 51.
11) A. V. Fedotov, I. Hofmann, R. L. Gluckstern and H. Okamoto: Phys. Rev. STAB **6** (2003) 094201.
12) R. C. Davidson and E. A. Startsev: Phys. Rev. STAB **7** (2004) 024401.
13) J. Struckmeier, J. Klabunde and M. Reiser: Part. Accel. **15** (1984) 47.
14) I. Bozsik and I. Hofmann: Nucl. Instrum. Methods Phys. Res., Sect. A **187** (1981) 305.
15) S. Machida: Nucl. Instrum. Methods Phys. Res., Sect. A **309** (1991) 43.
16) A. V. Fedotov, R. L. Gluckstern, S. S. Kurennoy and R. D. Ryne: Phys. Rev. STAB **2** (1999) 014201.
17) J. Qiang, R. D. Ryne, B. Blind, J. H. Billen, T. Bhatia, R. W. Garnett, G. Neuschaefer and H. Takeda: Nucl. Instrum. Methods Phys. Res., Sect. A **457** (2001) 1.
18) I. Hofmann, J. Qiang and R. D. Ryne: Phys. Rev. Lett. **86** (2001) 2313.
19) R. Cappi, R. Garoby, S. Hancock, M. Martini and J. P. Rinaud: Proc. Particle Accelerator Conf., Washington, D.C., 1993, p. 3570.
20) T. P. Wangler: *Proc. 20th ICFA Workshop, Fermilab* (AIP, New York, 2002).
21) C. K. Allen, K. C. D. Chan, P. L. Colestock, K. R. Crandall, R. W. Garnett, J. D. Gilpatrick, W. Lysenko, J. Qiang, J. D. Schneider, M. E. Schulze, R. L. Sheffield, H. V. Smith and T. P. Wangler: Phys. Rev. Lett. **89** (2002) 214802.
22) T. Uesugi, S. Machida and Y. Mori: Phys. Rev. STAB **5** (2002) 044201.
23) S. Cousineau, J. Holmes, J. Galambos, A. Fedotov, J. Wei and R. Macek: Phys. Rev. STAB **6** (2003) 074202.
24) L. R. Prost, P. A. Seidl, F. M. Bieniosek, C. M. Celata, A. Faltens, D. Baca, E. Henestroza, J. W. Kwan, M. Leitner, W. L. Waldron, R. Cohen, A. Friedman, D. Grote, S. M. Lund, A. W. Molvik and E. Morse: Phys. Rev. STAB **8** (2005) 020101.
25) H. Okamoto: Hiroshima Univ. Rep. HUBP-01/98, 1998.
26) H. Okamoto and H. Tanaka: Nucl. Instrum. Methods Phys. Res., Sect. A **437** (1999) 178.
27) R. C. Davidson, H. Qin and G. Shvets: Phys. Plasmas **7** (2000) 1020.
28) E. P. Gilson, R. C. Davidson, P. C. Efthimion and R. Majeski: Phys. Rev. Lett. **92** (2004) 155002.
29) P. G. O'Shea, M. Reiser, R. A. Kishek, S. Bernal, H. Li, M. Pruessner, V. Yun, Y. Cui, W. Zhang, Y. Zou, T. Godlove, D. Kehne, P. Haldemann and I. Haber: Nucl. Intrum. Methods Phys. Res., Sect. A **464** (2001) 646.
30) R. Takai, K. Ito, Y. Iwashita, H. Okamoto, S. Taniguchi and Y. Tomita: Nucl. Instrum. Methods Phys. Res., Sect. A **532** (2004) 508.
31) H. Okamoto, Y. Wada and R. Takai: Nucl. Instrum. Methods Phys. Res., Sect. A **485** (2002) 244.
32) W. Paul and H. Steinwedel: Z. Naturforsch. A **8** (1953) 448.
33) R. P. Ghosh: *Ion Traps* (Oxford Science, Oxford, 1995), and references therein.
34) F. Diedrich, E. Peik, J. M. Chen, W. Quint and H. Walther: Phys. Rev. Lett. **59** (1987) 2931.
35) H. C. Nägerl, Ch. Roos, D. Leibfried, H. Rohde, G. Thalhammer, J. Eschner, F. Schmidt-Kaler and R. Blatt: Phys. Rev. A **61** (2000) 023405.
36) M. G. Raizen, J. M. Gilligan, J. C. Bergquist, W. M. Itano and D. J. Wineland: Phys. Rev. A **45** (1992) 6493.
37) M. Drewsen, C. Brodersen, L. Hornekær, J. S. Hangst and J. P. Schifffer: Phys. Rev. Lett. **81** (1998) 2878.
38) J. I. Cirac and P. Zoller: Phys. Rev. Lett. **74** (1995) 4091.
39) T. Baba and I. Waki: Jpn. J. Appl. Phys. **35** (1996) L1134.
40) D. J. Berkeland, J. D. Miller, J. C. Bergquist, W. M. Itano and D. J. Wineland: Phys. Rev. Lett. **80** (1998) 2089.
41) K. Okada, M. Wada, T. Nakamura, R. Iida, S. Ohtani, J. Tanaka, H. Kawakami and I. Katayama: J. Phys. Soc. Jpn. **67** (1998) 3073.
42) N. Kjærgaard, K. Mølhave and M. Drewsen: Phys. Rev. E **66** (2002) 015401(R).
43) D. J. Wineland and H. Dehmelt: Bull. Am. Phys. Soc. **20** (1975) 637.
44) T. W. Hänsch and A. L. Schawlow: Opt. Commun. **13** (1975) 68.
45) K. Muraoka and M. Maeda: *Laser-Aided Diagnostics of Plasmas and Gases* (Institute of Physics Publishing, Bristol, 2001), and references therein.
46) See, for example, A. Chao: *Physics of Collective Beam Instabilities in High Energy Accelerators* (Wiley, New York, 1993).
47) Nobody has achieved Coulomb crystallization in a system with strong dispersion, whereas it is quite easy to form various bunched crystals in an ion trap. Extensive theoretical studies for the last decade have revealed how seriously dispersion and other effects peculiar to a storage ring can affect the dynamic motion of a crystalline beam.
48) German researchers have experimentally confirmed a dispersive instability of Coulomb crystals in a circular Paul trap: U. Schramm, M. Bussmann and D. Habs: Nucl. Instrum. Methods Phys. Res., Sect. A **532** (2004) 348.
49) D. R. Denison: J. Vac. Sci. Technol. **8** (1971) 266.
50) The MAFIA Collaboration: MAFIA Manual Version 4.024, CST GmbH, Darmstadt, 2000.
51) Note that the base potential *on axis* is not exactly equal to the voltage U_{IS} applied to the quadrupole electrodes.
52) The linearized Vlasov theory in ref. 6 predicts that the distribution of resonance stopbands for the sinusoidal confinement is almost identical to that for a FODO lattice with 50% filling (see Fig. 1).
53) Y. Wang, J. Franzen and K. P. Wanczek: Int. J. Mass Spectrom. Ion Processes **124** (1993) 125.
54) Y. Wang: Rapid Commun. Mass Spectrom. **7** (1993) 920.
55) J. L. Wiza: Nucl. Instrum. Methods **162** (1979) 587.
56) S. Matsuura, S. Umebayashi, C. Okuyama and K. Oda: IEEE Trans. Nucl. Sci. **31** (1984) 399.
57) T. Goto, K. Ishii, T. Takahashi, A. Abe, Y. Katsuki, N. Kikuno, Y. Goi, Y. Ono, N. Ishibashi, Y. Nakashima, K. Yatsu and T. Tamano: Jpn. J. Appl. Phys. **35** (1996) L738.
58) P. M. Shikhaliev: Nucl. Instrum. Methods Phys. Res., Sect. A **420** (1999) 202.
59) M. N. Gaboriaud, M. Desaintfuscien and F. G. Major: Int. J. Mass Spectrom. Ion Phys. **41** (1981) 109.
60) A. Kajita, M. Kimura, S. Ohtani, H. Tawara and Y. Saito: J. Phys. Soc. Jpn. **60** (1991) 2996.
61) K. Okada, M. Wada, T. Nakamura, I. Katayama, L. Boesten and S. Ohtani: Jpn. J. Appl. Phys. **40** (2001) 4221.
62) S. Urabe, J. Umezu and M. Ishizu: Oyo Buturi **54** (1985) 964 [in Japanese].
63) J. Yoda and K. Sugiyama: Jpn. J. Appl. Phys. **26** (1987) L1780.
64) M. Aramaki, Y. Sakawa, T. Shoji and K. Hayasaka: J. Plasma Fusion Res. **77** (2001) 284 [in Japanese].
65) T. Baba and I. Waki: J. Appl. Phys. **89** (2001) 4592.
66) M. Aramaki, Y. Sakawa, T. Shoji and K. Hayasaka: J. Plasma Fusion Res. **77** (2001) 476 [in Japanese].